Chemistry & Biology
Resource

An Engineered Monomeric *Zoanthus sp.* Yellow Fluorescent Protein

Hiofan Hoi,[1] Elizabeth S. Howe,[2] Yidan Ding,[1] Wei Zhang,[1] Michelle A. Baird,[2] Brittney R. Sell,[2] John R. Allen,[2] Michael W. Davidson,[2] and Robert E. Campbell[1,*]
[1]Department of Chemistry, University of Alberta, Edmonton, AB T6G 2G2, Canada
[2]National High Magnetic Field Laboratory and Department of Biological Science, Florida State University, 1800 East Paul Dirac Drive, Tallahassee, FL 32310, USA
*Correspondence: robert.e.campbell@ualberta.ca
http://dx.doi.org/10.1016/j.chembiol.2013.08.008

SUMMARY

Protein engineering has created a palette of monomeric fluorescent proteins (FPs), but there remains an ~30 nm spectral gap between the most red-shifted useful *Aequorea victoria* green FP (GFP) variants and the most blue-shifted useful *Discosoma sp.* red FP (RFP) variants. To fill this gap, we have engineered a monomeric version of the yellow FP (YFP) from *Zoanthus sp.* coral. Our preferred variant, designated as mPapaya1, displays excellent fluorescent brightness, good photostability, and retains its monomeric character both in vitro and in living cells in the context of protein chimeras. We demonstrate that mPapaya1 can serve as a good Förster resonance energy transfer (FRET) acceptor when paired with an mTFP1 donor. mPapaya1 is a valuable addition to the palette of FP variants that are useful for multicolor imaging and FRET-based biosensing.

INTRODUCTION

Past efforts to fill the toolbox of fluorescent proteins (FPs) with bright, photostable, monomeric variants that have fluorescence excitation and emission spectra ranging from the blue to far-red regions of the visible spectrum have been a resounding success. Accordingly, the research community now has a palette of FPs that can be used in a multitude of combinations for multicolor and FRET imaging experiments. Arguably, the most notable shortcoming of the currently available palette of monomeric FPs that are most useful for imaging is an unfilled spectral gap in the yellow region (~530 nm to ~560 nm) of the visible spectrum. Bracketing the lower wavelength end of this spectral gap are two of the most useful red-shifted *Aequorea* GFP variants, Venus (λ_{em} = 528 nm) (Nagai et al., 2002) and Citrine (λ_{em} = 529 nm) (Griesbeck et al., 2001), which both harbor the key threonine to tyrosine substitution at position 203 (Table S1 available online). This substitution causes a 20 nm red-shift in the excitation and emission spectra relative to wild-type GFP, presumably due to a π-π interaction between the aromatic side chain of Tyr203 and the phenolic ring in the chromophore (Ormö et al., 1996). Bracketing the longer wavelength end of this spectral gap are mOrange2 (λ_{em} = 565 nm) derived from *Discosoma* RFP (Shaner et al., 2008) and mKO (λ_{em} = 559 nm) derived from an FP cloned from the stony coral *Fungia concinna* (Karasawa et al., 2004).

There are a small number of engineered and wild-type FPs with emission in the yellow spectral gap, but none of them are optimal for live cell imaging experiments. For example, the engineered RFP-derived mHoneydew (λ_{em} = 537 nm) and mBanana (λ_{em} = 553 nm) variants are monomeric but are not considered to be practically useful due to their dim fluorescence and poor photostability (Shaner et al., 2004, 2005). Wild-type proteins with similar yellow hues include phiYFP (λ_{ex} = 525 nm; λ_{em} = 537 nm) from the hydromedusa *Phialidium sp.* (Shagin et al., 2004), and zFP538 (λ_{ex} = 528; λ_{em} = 538 nm) from button polyp *Zoanthus sp.* (Matz et al., 1999). The phiYFP chromophore is red-shifted relative to GFP due to a π-π stacking interaction analogous to that found in the GFP-derived YFPs and additional hydrogen bonding interactions between the β-barrel and the chromophore (Pakhomov and Martynov, 2011). In contrast, zFP538 possess a unique three-ring chromophore (Figure 1A, inset) formed from the amino acid triad Lys66-Tyr67-Gly68, as determined by a combination of mass spectrometry and X-ray crystallographic studies (Zagranichny et al., 2004; Remington et al., 2005). Following the formation of a typical RFP-type chromophore, the N_ξ of Lys66 participates in a transimination reaction to replace the acylimine C_α = N bond at position 66, leading to the formation of a six-member heterocyclic ring and the breakage of the peptide backbone (Remington et al., 2005).

Due to its distinct emission in the yellow spectral gap and its intriguing chromophore structure that could serve as an entry point to a new subclass of FP variants with unique properties, we decided to undertake the engineering of zFP538 for improved performance in live cell imaging applications. We anticipated that the major barrier to achieving this goal would be engineering a monomeric variant of the tetrameric FP (Figure 1A). A tetrameric zFP538 variant that does not aggregate in higher order complexes has previously been reported (Yanushevich et al., 2002). It is widely accepted in the field of FP imaging that a monomeric quaternary structure is required for a FP to be practically useful as a fluorescence tag or FRET partner.

RESULTS AND DISCUSSION

Expression and Initial Engineering of Codon-Optimized zFP538

We designed and synthesized a mammalian codon usage optimized version of the zFP538. To facilitate later subcloning with

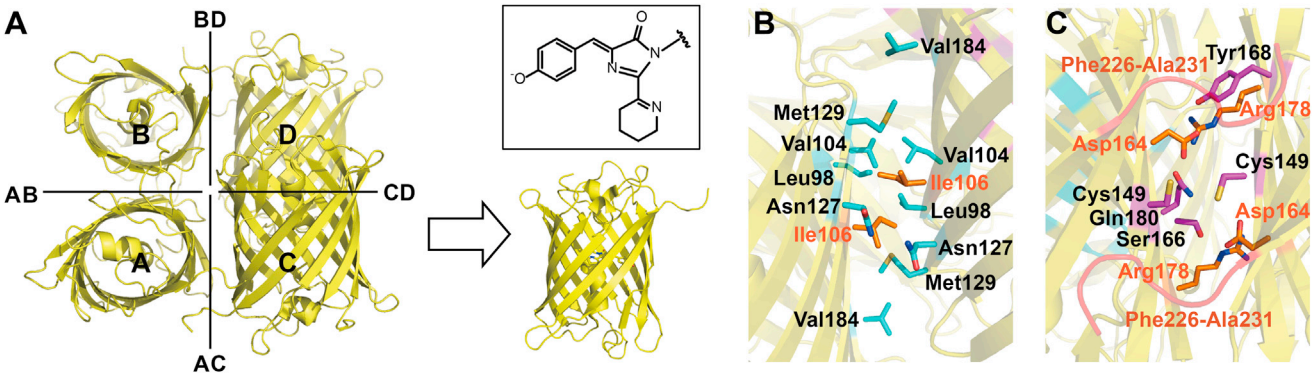

Figure 1. Interface Disruption Converts an FP from a Tetramer to a Monomer

(A) Schematic representation of the overall monomerization process. Shown is the tetrameric structure of zFP538 (Protein Data Bank [PDB] ID 2OGR; Remington et al., 2005) with the subunits of the tetramer labeled A through D. The BD and AC interfaces are equivalent, as are the AB and CD interfaces. Inset is the zFP538 chromophore structure.

(B) Closeup on the hydrophobic antiparallel interface (AB and CD). Key residues are highlighted in red.

(C) The hydrophilic perpendicular interface (AC and BD) represented as in (B). The side chains of key residues and the main chain for residues 226–231 are highlighted in red.

common FP primers, we replaced the first two residues (Met and Ala) with the *Aequorea* GFP N-terminal sequence (Met-Val-Ser-Lys-Gly-Glu-Glu), and appended the GFP C-terminal sequence Met-Asp-Glu-Lys-Tyr-Lys to its C terminus. Expression of this modified zFP538 gene in *Eshcherichia coli* resulted in yellow fluorescent colonies. Screening of a gene library, created by error-prone PCR and expressed in colonies of *E. coli,* resulted in the discovery of the brightness-enhancing mutation Met129Val (Figure 2A). This mutation is also present in the commercially available zFP538 variant, known as ZsYellow1 (Clontech). Because the color of the purified zFP538-M129V with GFP-derived termini is very close to that of papaya fruit when viewed in white light (Figure 2E, inset), we named this variant as tetrameric Papaya version 0.01 (tPapaya0.01). Gel filtration chromatography of purified tPapaya0.01 protein revealed that it exists as a mixture of a tetrameric species (peak at 58 ml) and a higher order oligomer (peak at 39 ml; Figure 2B).

Interface Disruption of tPapaya0.01

The most commonly used strategy to develop monomeric FPs from tetrameric precursors is to use mutagenesis to switch formerly stabilizing intersubunit interactions into repulsive interactions. This approach relies on a combination of rational protein engineering and directed evolution and has been successfully used with a growing number of FPs (Campbell et al., 2002; Karasawa et al., 2004; Ai et al., 2006; Gurskaya et al., 2006; Ilagan et al., 2010; Shaner et al., 2013). Given these past examples, we expected that it would be possible to engineer a monomeric variant of zFP538 using a similar strategy.

The X-ray crystal structure of zFP538 (Figure 1A) reveals that there are two distinct interfaces in the zFP538 tetramer (Remington et al., 2005; Pletneva et al., 2007): the antiparallel interface between subunits A and B (equivalent to the CD interface; see Figure 1B) and the perpendicular interface between subunits A and C (equivalent to the BD interface; see Figure 1C). Stabilizing interactions at the antiparallel interface (AB and CD) generally involve interactions between residues with hydrophobic side chains (Figure 1B; Remington et al., 2005). In contrast, the interactions at the perpendicular interface (AC and BD) are generally hydrophilic and more extensive and diverse in nature than the interactions at the antiparallel interface (Remington et al., 2005). Altogether, eight hydrogen bonds, four salt bridge interactions, and a number of hydrophobic interactions, which largely involve approximately the last ten residues at the C terminus of the protein, are observed at the AC and BD interfaces (Figure 1C; Remington et al., 2005).

In an effort to generate a monomeric variant of Papaya, we attempted to disrupt the simpler AB interface by mutating Ile106 to both Arg and Lys (Figures 1B and 2A) under error-prone PCR conditions. The brightest yellow fluorescent variant in this library harbored Ile106Arg plus the additional mutation Val115Glu, and was substantially dimmer than tPapaya0.01. The gel filtration chromatography elution profile of this variant, designated as dPapaya0.1, confirmed that the protein was primarily a dimer (Figure 2B). To disrupt the remaining AC interface, we simultaneously mutated Asp164 to both Arg and Lys and Arg178 to Asp, Asn, Lys, His, Gln, and Glu. The brightest variant (mPapaya0.2) in this small library, which was nevertheless extremely dim when expressed in colonies of *E. coli*, was found to harbor Asp164Lys and Arg178His.

Directed Evolution of mPapaya for Improved Brightness and Monomeric Structure

In an attempt to restore the brightness lost during monomerization, we performed four successive rounds of directed evolution by creating libraries using random mutagenesis and screening for brightness. This effort led to mPapaya0.27, which had seven additional mutations (Figure 2A) and displayed reasonable fluorescence in *E. coli* after overnight incubation at 37°C. Analysis of the purified protein by gel filtration chromatography revealed that the elution profile had peaks at 72 ml and 65 ml with a shoulder at 58 ml (Figure 2B). Control experiments using size standards indicated that the peak at 72 ml corresponded to the monomeric species, the peak at 65 ml to the dimeric species, and the shoulder at 58 ml to the tetramer. This promising result indicated to us that mPapaya0.27 existed as a slowly equilibrating mixture of

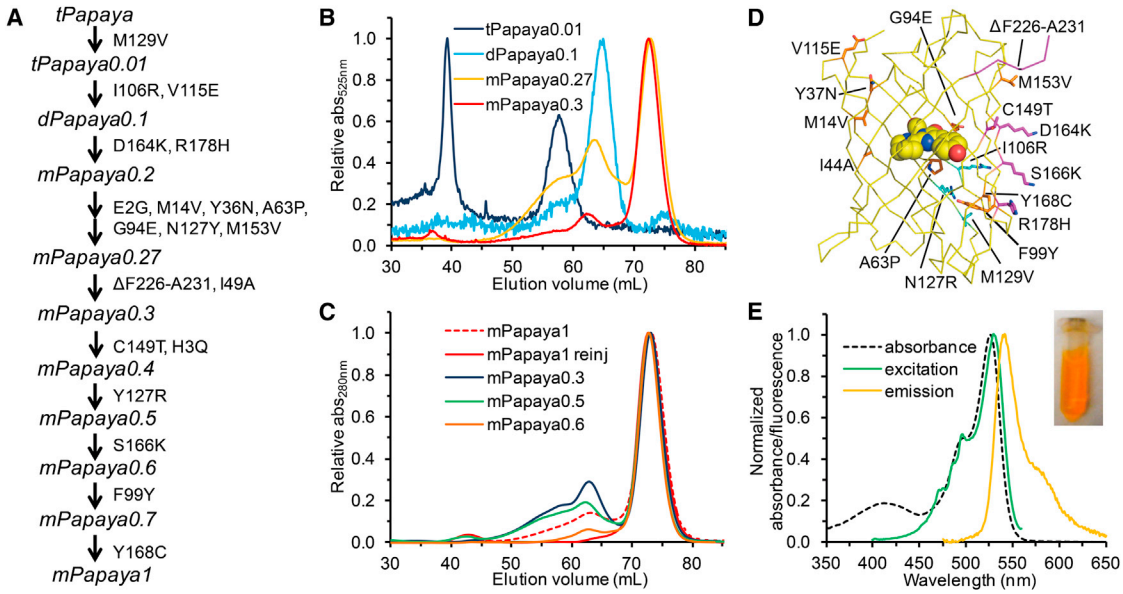

Figure 2. Engineering a Monomeric Variant of zFP538

(A) Lineage of mPapaya1.

(B) Gel filtration chromatography profiles of early Papaya variants with the absorbance of the eluent monitored at 525 nm. The monomeric FP mCherry eluted at 72 ml and the dimeric FP dTomato eluted at 67 ml.

(C) Gel filtration profiles of later Papaya variants when the absorbance of the eluent is monitored at 280 nm. mPapaya0.3 has a significant peak at 65 ml with a shoulder at 53 ml. The dimer peak and tetramer shoulder are gradually reduced in subsequent variants.

(D) Locations of substitutions that were introduced during the directed evolution process. Mutations E2G and H3Q are not shown. The coordinates of zFP538 (PDB ID 2OGR, chain A) are used in this representation (Remington et al., 2005).

(E) Spectral characterization of mPapaya1. Inset shows a purified sample of the protein under white light illumination.

See also Figure S1 and Table S2.

monomers, dimers, and tetramers. Such an equilibrium would be expected to be concentration dependent, with higher concentrations favoring the higher order oligomers.

Because the last ten residues at the C terminus of zFP538 form a large part of the AC and BD interfaces (Remington et al., 2005), we deleted the six residues from position 226 to 231 (Figure 1C). Although this modification resulted in decreased fluorescent brightness, one round of directed evolution led to the identification of mPapaya0.3, which was similar in brightness to its mPapaya0.27 parent. The gel filtration chromatography elution profile of mPapaya0.3 (monitored at 525 nm) revealed that the dimeric (and higher order) character was greatly reduced and that it predominantly exists as a monomer (Figure 2B). However, when the gel filtration chromatography elution profile was monitored at 280 nm, a wavelength at which all proteins absorb and is therefore a measure of total protein concentration, we found that a portion of mPapaya0.3 eluted at 53 ml and 62 ml (Figure 2C), suggesting the presence of immature (i.e., lacking a properly formed chromophore) tetrameric and dimeric oligomers, respectively. Apparently, these oligomeric forms are sufficiently folded and soluble to be purified by affinity chromatography. We were concerned that the presence of these nonfluorescent oligomers could contribute to increased cytotoxicity, or potentially interfere with the function and behavior of the protein of interest, when mPapaya was used as a fusion tag.

To further diminish the oligomeric character of mPapaya, we undertook additional engineering of the former protein-protein interfaces. Close inspection of the X-ray crystal structure of zFP538 (Remington et al., 2005) led us to suspect that the weak oligomerization tendency could be due to the individual or cooperative result of the following interactions: Leu98(A)-Leu98(B), Val104(A)-Val104(B), Tyr127(A)-Tyr127(B), Val131(A)-Val131(B), Cys149(A)-Cys149(C) or Ser166(A)-Lys164(C). Accordingly, each of the above positions was mutated into Lys/Arg or Thr/Ser by site-directed mutagenesis (Table S2) and the purified proteins were examined by gel filtration chromatography. Ultimately, we found the remaining oligomerization tendency was successfully abolished in mPapaya0.3 with mutations Tyr127Arg, Cys149Thr, and Ser166Lys (designated mPapaya0.6), without any substantial loss of brightness. Of the three mutations, Ser166Lys is the main contributor to the decrease in oligomerization tendency based on the gel filtration chromatography elution profiles (Figure 2C). In the crystal structure of zFP538, Ser166 and Asp164 are engaged in a hydrogen bonding interaction across the AC interface (Figure 1C). In mPapaya0.6, this stabilizing interaction has been replaced with a repulsive interaction between the positively charged side chains of Ser166Lys and Asp164Lys, which was introduced earlier in the engineering.

Engineering Improved Photostability

A drawback of mPapaya0.6 that soon became apparent was relatively poor photostability under typical live cell imaging conditions. Similar to mTFP0.7, photobleached mPapaya0.6 displayed a 410 nm absorbance peak attributable to the protonated state of the chromophore and was observed to recover fluorescence when stored in the dark (Henderson et al., 2007). These

Table 1. Properties of mPapaya1 and ZsYellow1

Protein	λ_{exc} (nm)	λ_{em} (nm)	ε[a]	Φ	Brightness[b]	pK_a	Oligomeric Structure
mPapaya1	530	541	43	0.83	36	6.8	monomer
mPapaya0.7	529	541	28	0.69	19	6.8	monomer
ZsYellow1[c]	529	539	20	0.65	13	ND	tetramer

ND, not determined. See also Table S1 and Figure S3.
[a]Unit of mM^{-1} cm^{-1}.
[b]Product of ε and Φ in mM^{-1} cm^{-1}.
[c]Data from Clontech website (http://www.clontech.com/).

results indicated that the poor photostability was a reversible photoswitching phenomenon possibly attributable to photoisomerization of the chromophore. Because we have previously been successful at engineering improved photostability from a photoswitching variant (Ai et al., 2006), we decided to undertake additional directed evolution of mPapaya variants for improved photostability. Libraries of mPapaya variants expressed in *E. coli* colonies were illuminated with 6.5 mW/cm^2 of 510–560 nm light for 30 min, then imaged to find the brightest colonies. We constructed a number of targeted libraries in which various positions in proximity to the chromophore (i.e., positions 44, 62, 63, 163, 165, and 167) were randomized individually or in combination (Table S2). Thorough screening of these libraries did not lead to the identification of variants with improved photostability. However, parallel efforts to screen libraries produced by error-prone PCR did lead to the discovery of mPapaya0.7 with the Phe99Tyr mutation that dramatically improved the photostability under the screening conditions. Further screening led to the identification of the Tyr168Cys mutation that was associated with a 1.6-fold increase in the extinction coefficient (from 28 to 43 mM^{-1} cm^{-1}) and a 1.2-fold increase in the quantum yield (from 0.69 to 0.83; Table 1). This variant was designated as mPapaya1.

In Vitro Characterization of mPapaya1

Relative to zFP538, mPapaya1 has 18 point mutations in addition to the deletion of residues 226–231 and the appended *Aequorea*-type termini (Figures 2D and S1). Despite this large number of changes, mPapaya1 and zFP538 have very similar excitation maxima (530 nm and 529 nm, respectively) and emission maxima (541 nm and 539 nm, respectively) (Figure 2E; Table 1). The absorbance spectrum of mPapaya1 reveals a non-excitable absorbance peak at 415 nm, which is attributable to the protonated state of the chromophore (Figure 2E), and is consistent with its relatively high fluorescence pK_a of 6.8 (Hill coefficient of 0.89; Figure S3). The high pK_a of mPapaya1 will limit the utility of this protein for labeling of acidic organelles, but may prove useful for monitoring of subcellular pH changes. Looking back at earlier generations of mPapaya, an absorbance peak for the protonated state was not apparent until Cys149Thr was introduced at the stage of mPapaya0.4. Indeed, mPapaya0.3 has a lower pK_a of 6.4. In an attempt to lower the pK_a of mPapaya1, we replaced Thr149 with Ser, Val, and Ala. Unfortunately, the pK_a of both Thr149Ser and Thr149Ala remained 6.8, while Thr149Val exhibited much dimmer fluorescence. Despite its higher pK_a, mPapaya1 has 280% of the brightness of ZsYellow1 at physiological pH (Table 1). The increased brightness is largely attributed to an increased extinction coefficient.

To determine the photostability of mPapaya1, the purified protein was immobilized by embedding a 1 μM solution in a 20% acrylamide/bis-acrylamide gel that was polymerized between a glass slide and a coverslip. The glass slide was then placed on the stage of microscopes equipped with three different light sources, and the photobleaching half-time determined as a function of power (Figures S2A–S2F). We determined that, even at matched powers, the absolute rate of photobleaching depends on the light source used. As expected, under all conditions mPapaya1 is more photostable than mPapaya0.6. The difference in photostability is most apparent when using an LED light source at powers comparable to those used for screening for improved photostability. When using a mercury arc lamp or confocal laser illumination, mPapaya1 has a photostability that is comparable to or better than that of the popular YFPs mVenus (Nagai et al., 2002) and mCitrine (Griesbeck et al., 2001).

Validation of mPapaya1 as a Monomer under Physiological Conditions

Although the elution profile of mPapaya1 shows that it exists as a monomer in vitro, we were concerned it might still oligomerize under certain physiological conditions as has been observed for certain FPs that were claimed to be monomeric (Costantini et al., 2012). To test the monomeric character under physiological conditions with a "challenging" chimera, we constructed CytERM-mPapaya1. CytERM is an endoplasmic reticulum (ER) signal-peptide that anchors its C-terminally fused protein partner to the cytoplasmic side of ER (Snapp et al., 2003). Even relatively low affinity oligomeric interactions between FPs fused to CytERM can serve to restructure the tubular ER structure into stacked membrane arrays that appear as bright whorl-like structures (Figures S2G–S2J; Costantini et al., 2012). To exploit this phenomenon for assessing the monomeric character of a FP, we determined the percentage of transfected HeLa (CCL-2; ATCC) cells that are whorl-free. This analysis revealed that 87.6% ± 3.2% of mPapaya1 and 95.1% ± 1.1% of mPapaya0.6-expressing cells were whorl-free. These values compare favorably with enhanced GFP, which had 76.5% ± 6.9% of cells whorl-free, and are very similar to the values of 83.9% ± 4.4% and 93.8% ± 2.6% obtained for mVenus and mCitrine (both with the monomerizing mutation Ala206Lys), respectively (Zacharias et al., 2002).

Performance of mPapaya1 Targeting Fusions

Tetrameric fluorescent proteins, such as the commercially available ZsYellow1 and DsRed2 (Clontech), perform very poorly in targeting fusions, usually leading to the production of large intracellular aggregates and ultimately cell death. To gauge the

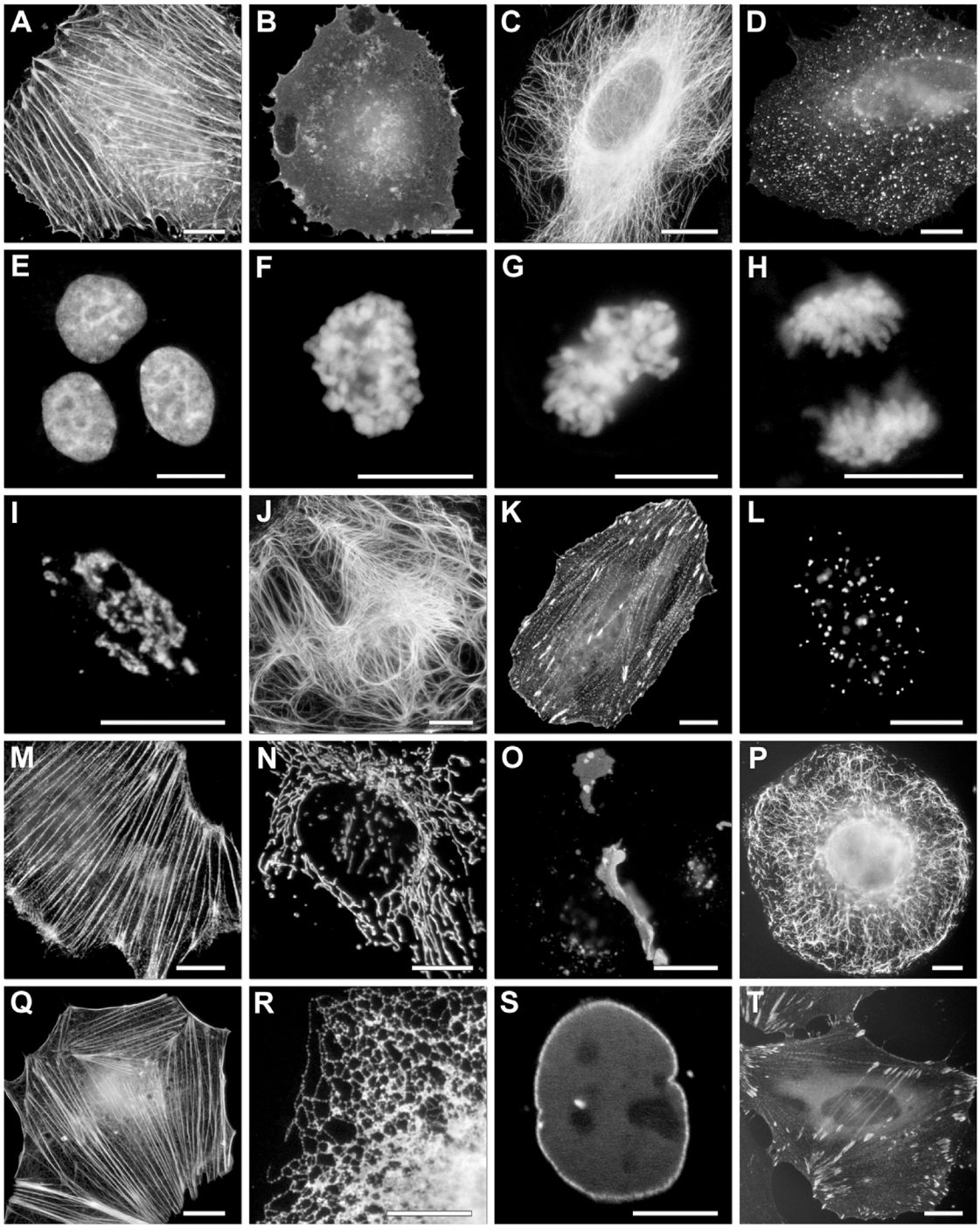

Figure 3. Fluorescence Imaging of Representative mPapaya1 Fusions

(A–H), Fusions to the C terminus of Papaya1 are shown. For each fusion, the amino acid length of the linker between mPapaya1 and the targeting cDNA is presented after the fusion construct name. Similar results were obtained with mPapaya0.6. Scale bars represent 10 μm. Fusions include: (A) mPapaya1-β-actin-C-18 (human; target: actin cytoskeleton); (B) mPapaya1-CAAX-C-5 (20-amino acid farnesylation signal from c-Ha-Ras; target: plasma membrane); (C) mPapaya1-α-tubulin-C-18 (human; target: microtubules); (D) mPapaya1-Rab4a-C-7 (human; target: endosomes); and (E–H) mPapaya1-H2B-C-10 (human; target: nucleosomes) during (E) interphase, (F) prophase, (G) metaphase, and (H) anaphase.

(I–T) Fusions to the N terminus of Papaya1 using the same nomenclature as (A–H). Fusions include: (I) mPapaya1-MANNII-N-10 (mouse mannosidase 2; target: Golgi apparatus); (J) mPapaya1-Keratin-N-17 (human; target: intermediate filaments); (K) mPapaya-α-actinin-N-19 (human non-muscle; target: actin and focal adhesions); (L) mPapaya1-CENP-B-N-22 (human; target: centromeres); (M) mPapaya1-LC-Myosin-C-7 (mouse; target: cytoskeleton); (N) mPapaya1-PDHA1-N-10 (human pyruvate dehydrogenase; target: mitochondria); (O) mPapaya1-Cx43-N-7 (rat α-1 connexin 43; target: gap junctions); (P)

(legend continued on next page)

performance of mPapaya1 as a live-cell imaging probe, we constructed a number of N- and C-terminal fusion proteins (Figure 3). In all cases, the expected localization patterns were observed, and this included three fusions that require a very high degree of monomeric character: α-tubulin (Figure 3C), connexin 43 (Figure 3O), and histone H2B fused to the C terminus of mPapaya1 (Figures 3E–3H). Overall, the high quality of localization exhibited by these mPapaya1 fusions indicates that they will be of use in a variety of live-cell imaging assays.

mPapaya1 as a FRET Acceptor for an mTFP1 Donor

One of our primary motivations for engineering a monomeric version of zFP538 was its potential to serve as a FRET acceptor for an mTFP1 donor (Ai et al., 2006). The calculated Förster radius (R_o) of the mTFP1-mPapaya1 FRET pair (R_o = 5.1 nm) is somewhat lower than that for mTFP1-mCitrine (R_o = 5.7 nm; Ai et al., 2006) but comparable to the commonly used ECFP-EYFP pair (R_o = 4.9 nm; Patterson et al., 2000). To experimentally determine if mTFP1 and mPapaya1 were a useful FRET pair, we fused the genes for the two fluorescent proteins via an 11-residue linker that contained a DEVD caspase-3 cleavage site. In vitro characterization of the purified protein revealed that mPapaya1 exhibited strong sensitized emission that disappeared when the linker region was proteolyzed, giving a 47.7% reduction (from 0.88 to 0.46) in acceptor to donor ratio (Figure 4C). These results were verified in mammalian cells by transient transfection and FRET imaging of cells undergoing apoptosis (Figure 4A and 4B and Figure S4). As expected, the FRET emission ratio reliably decreased by 29.5% ± 5.5% (n = 10) when caspase-3 was activated. Parallel experiments with mPapaya0.6 revealed substantially smaller ratio changes both in vitro (29.2%; from 0.65 to 0.46) and in cells (17.5% ± 3.8%; n = 7), indicating that the improved brightness of mPapaya1 was essential for its utility as a FRET acceptor.

A cameleon-type Ca^{2+} indicator (Miyawaki et al., 1997) based on the mTFP1 and mPapaya1 FRET pair was also tested; however, it was found to give relatively small Ca^{2+}-dependent ratio changes (11% increase in acceptor-to-donor ratio). As we have previously found when switching FRET pairs in a previously optimized FRET construct, extensive re-optimization will likely be required to improve the Ca^{2+} response to a useful level (Ding et al., 2011).

SIGNIFICANCE

The mPapaya1 protein is a useful monomeric FP that combines good brightness and photostability with a true yellow fluorescence maximum at 541 nm. Accordingly, mPapaya1 fills the spectral gap between monomeric GFP-derived YFPs and monomeric RFP-derived orange FPs, and effectively completes the FP coverage of the visible spectrum. The availability of mPapaya1 will create new opportunities for multicolor imaging of fusion protein localization and FRET-based biosensing. As we have demonstrated by creating and imaging a number of typical FP fusions, including some that are notoriously challenging, mPapaya1 is readily amenable to live cell imaging of subcellular protein localization. In all cases attempted to date, mPapaya1 chimeras have given localization patterns that are similar to those achieved with analogous monomeric EGFP chimeras, indicating that mPapaya1 does not interfere with the proper trafficking and localization of its fusion partner. Some drawbacks of mPapaya1 are that it is sensitive to physiologically relevant changes in pH and that it exhibits poor photostability with LED excitation. As a FRET partner, mPapaya1 could potentially be used either as a donor to a red FP or as an acceptor from a cyan or teal FP. Because we were particularly interested in the latter scenario, we assessed the performance of a caspase-3 FRET-based sensor based on an mTFP1 donor and mPapaya1 acceptor. This mTFP1-DEVD-mPapaya1 construct was found to give excellent ratiometric changes upon cleavage both in vitro and in apoptotic cells.

EXPERIMENTAL PROCEDURES

General Methods and Materials

All synthetic DNA oligonucleotides for cloning and library construction were purchased from Integrated DNA Technologies. Taq (New England Biolabs) and Pfu polymerases (Fermentas) were used for error-prone PCR or standard PCR, respectively. PCR products and products of restriction digests were purified using QIA gel extraction kit (QIAGEN) or GeneJET gel extraction kit (Fermentas) according to the manufacturer's protocols. Restriction enzymes were purchased from New England Biolabs or Fermentas. The cDNA sequences were confirmed by dye terminator cycle sequencing using the DYEnamic ET kit (GE Life Sciences) or BigDye Terminator v3.1 Cycle Sequencing Kit (Applied Biosystems - Invitrogen). Sequencing reactions were analyzed at the University of Alberta Molecular Biology Service Unit or the Florida State University Department of Biological Science DNA Sequencing Facility.

Plasmid Library Creation and Screening

For plasmid library creation, general molecular biology procedures were performed as previously described (Hoi et al., 2010). Saturation or semisaturation mutagenesis at specific residues was performed using overlap extension PCR or QuikChange Site-Directed Mutagenesis Kit (Agilent Technologies). *E. coli* libraries were screened for brightness using a custom built imaging system (Cheng and Campbell, 2006) equipped with a 490–510 nm filter for excitation and a 520–550 nm filter for emission.

Protein Purification and Characterization

Protein purification, pH titrations, spectral characterization, and gel filtration chromatography were performed as previously described (Hoi et al., 2010). The extinction coefficient was calculated by dividing the absorbance by the protein concentration, which was determined by BCA protein assay kit (Pierce). The yellow FP mCitrine (Φ = 0.76) was used as the reference for quantum yield determination (Griesbeck et al., 2001). In vitro proteolysis of the FRET construct (0.5 μM) was performed with 0.1 μg/ml trypsin (Sigma T1426) in TBS pH 7.4. Spectra were acquired using a 384-well microplate reader (Tecan Safire2).

Construction of Mammalian Expression Plasmids

mPapaya1 targeting constructs were assembled using C1 and N1 (Clontech style) cloning vectors. The mPapaya1 cDNA was PCR amplified using a 5′

mPapaya1-vimentin-N-7 (human; target: intermediate filaments); (Q) mPapaya1-Lifeact-N-7 (yeast nucleotide sequence; target: actin); (R) mPapaya1-Calnexin-N-14 (human; target: endoplasmic reticulum); (S) mPapaya1-Nup50-N-10 (human; target: nuclear pore complex); and (T) mPapaya1-Zyxin-N-6 (human; target: focal adhesions).
See also Figure S2.

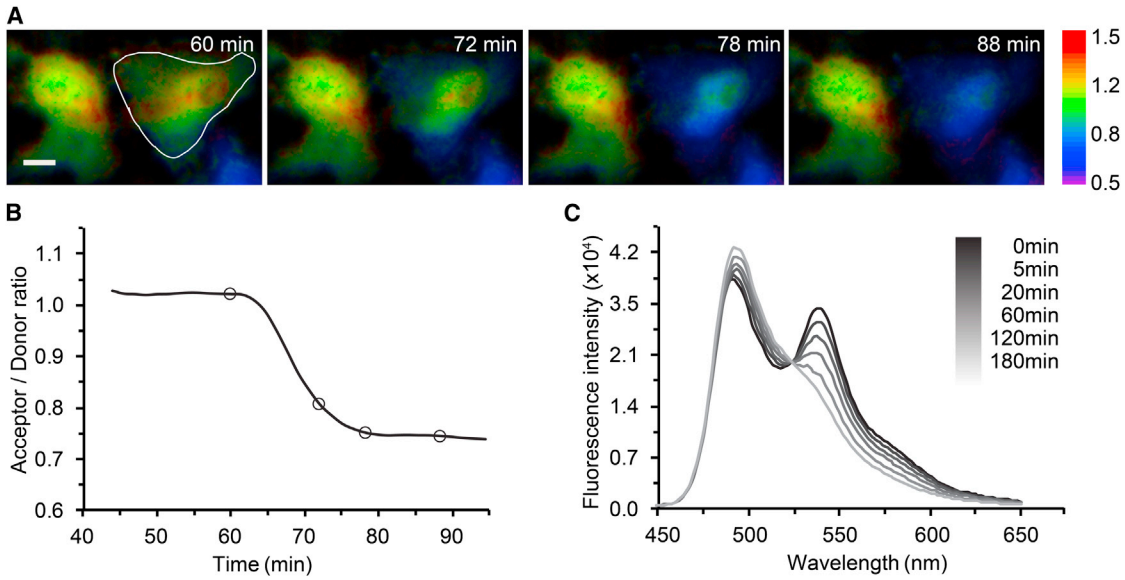

Figure 4. mPapaya1 as a FRET Acceptor from an mTFP1 Donor

(A) Selected frames from ratiometric imaging (acceptor/donor emission ratio) of staurosporine-treated HeLa cells expressing mTFP1-DEVD-mPapaya1. Scale bar represents 10 μm.

(B) Emission ratio versus time for the cell indicated in (A). The x axis is time elapsed since cells were treated with staurosporine to induce apoptosis. Time points corresponding to the frames in (A) are represented as open circles.

(C) In vitro proteolysis of mTFP1-DEVD-mPapaya1. A sample of the purified protein was treated with trypsin and fluorescence emission spectra were recorded at the times indicated.

See also Figure S4.

primer containing an AgeI site and a 3′ primer encoding either a BspEI (C1) or NotI (N1) site to create cloning vector fusions to the C and N terminus (with regards to the FP). The PCR products were gel purified, digested, and ligated to EGFP-C1 or EGFP-N1 vector backbones that had been similarly purified and digested. Assembled plasmids were amplified in *E. coli* and purified using a Maxi kit (QIAGEN). Cultures of HeLa (CCL-2 or CCL-2.2, ATCC) and PtK2 rat kangaroo (CCL-56, ATCC) cells (obtained from the ATCC, Manassas, VA) were transfected with approximately 1 μg of DNA per dish using Effectene (QIAGEN). Approximately 48 hr after transfection, the cells were fixed, mounted, and imaged to verify proper localization and expression of the plasmids.

To construct the vectors used for the OSER assay, the first 29 amino acids of rabbit cytochrome p450 (CytERM; XM_002718526.1) were inserted into a mEGFP-N1 vector. Genes encoding FPs were inserted downstream of the sequence encoding the p450 transmembrane segment using a 17 amino acid linker (RILQSTVPRARDPPVAT).

To construct mTFP1 and mPapaya FRET constructs for mammalian expression, the gene for mTFP1 was amplified with a 5′ primer with an XhoI site and a 3′ primer containing the coding sequence for the linker (SGSGDEVDGGT) and a KpnI site. The 5′ primer did not include the codon for the last residue of mTFP1, the protein ended with MDELY rather than MDELYK. mPapaya was amplified by a 5′ primer with a KpnI site and 3′ primer with a HindIII site. The purified PCR products were then digested and ligated through three-parts ligation into pcDNA3.1(+) (Life Technologies).

Fluorescence Microscopy

Imaging and photobleaching of mPapaya1 and its fusions was conducted using a customized filter block with a 494/41 nm excitation filter, 571/72 nm emission filter, and 525 nm CWL dichroic mirror (Semrock). HeLa or PtK2 cells were cultured in a 50:50 mixture of Dulbecco's modified Eagle's medium (DMEM) and Ham's F12 with 12.5% (v/v) Cosmic calf serum (Thermo Scientific) and transfected with Effectene (QIAGEN). Imaging was performed in Delta-T culture chambers (Bioptechs) under a humidified atmosphere of 5% CO_2 in air. Routine examination of living cells expressing constructs was performed with a Nikon TE-2000 inverted microscope equipped with a Photometrics Cascade II camera system. Laser-scanning confocal microscopy was conducted using an Olympus FV1000, equipped with argon-ion (457 and 488 nm) and helium-neon (543 nm) lasers and proprietary filter sets. Cell cultures expressing fluorescent protein fusions were fixed in 2% (w/v) paraformaldehyde (Electron Microscopy Sciences) and washed several times in PBS containing 0.05 M glycine before mounting with a polyvinyl alcohol water-based medium. Proper localization in all fusion constructs was confirmed by imaging fixed cell preparations on coverslips using a Nikon 80i microscope coupled to a Hamamatsu Orca ER camera. HeLa CCL2 cells were used for localization images in Figure 3, with the exception of panels E–H, P, and S (HeLa S3 cells) and panels J, M, and Q (PtK2 cells).

For ratiometric live cell imaging, HeLa cells in 35 mm imaging dishes were incubated with 1 ml DMEM (FBS free) for 10 min and then transfected with 1 μg of plasmid DNA that had been mixed with 2 μl of Turbofect (Fermentas) in 0.1 ml of DMEM (FBS free). The culture media was changed back to DMEM with 10% FBS after 2 hr incubation at 37°C. Apoptosis was initiated by treatment with the nonspecific kinase inhibitor staurosporine with the final concentration of 2 μM (Ding et al., 2011). Cells were maintained in HEPES-buffered Hank's balanced salt solution (HHBSS) and subjected to imaging at 1 or 2 min intervals for 4-6 hr. FRET imaging was performed on an inverted Nikon Eclipse Ti microscope equipped with a 75 W xenon lamp (OSRAM), a 60× objective (NA = 1.4) and a 16-bit 512SC QuantEM CCD (Photometrics). Exposure times were adjusted between 200 ms to 400 ms to obtain suitable intensities in each channel. Filter sets were identical to those used previously for FRET imaging of the mTFP1-mCitrine FRET pair (Ding et al., 2011). Background subtraction was performed for both the donor and acceptor channels using the average intensity for a cell-free area of interest adjacent to the cell being imaged. Ratios (R) were calculated by dividing the background-corrected intensity of the acceptor channel by the background-corrected intensity of the donor channel. Ratio changes expressed as percent were calculated as $100 * (R_{initial} - R_{final})/R_{initial}$.

Photobleaching

Photobleaching experiments were performed on glass slides mounted with a 22 × 50 mm coverslip on top of two spacer coverslips that were placed

~1.5 cm apart. A 20% acrylamide/bis-acrylamide solution containing 1 μM of mPapaya1 was prepared, catalyzed, and then pipetted directly underneath the large coverslip. Following polymerization, the coverslips were sealed with Cytoseal (Richard-Allan Scientific) to prevent dehydration of the gel and imaged less than 24 hr after mounting. Widefield metal halide and LED photobleaching were performed on a Nikon TE2000 inverted microscope, equipped with a Nikon Plan Fluorite 60× oil immersion objective (NA = 1.25) and an X-Cite eXacte metal halide lamp (Lumen Dynamics) or X-Cite XLED1 light engine (Lumen Dynamics). A Newport 1918-C (Newport) optical power meter was used to measure multiple illumination powers at the objective. Power moderation was achieved by using neutral density filters contained within the lamp. With a high-level neutral density filter (ND32) in the optical pathway, an evenly illuminated area of the gel was identified, at which point new areas in the same plane could be chosen for photobleaching. Once a region was chosen for photobleaching, the neutral density was removed and the region was photobleached continuously until it reached less than 50% of its initial starting intensity. Images were collected with a QImaging Retiga EXi camera (Photometrics). Raw data from 20 repetitions of the experiment was collected using NIS-Elements software (Nikon) and exported to Excel (Microsoft) for processing.

Confocal photobleaching measurements were similarly conducted on an Olympus FV1000 microscope (Olympus) with an Olympus PlanApo 60× oil-immersion objective (NA = 1.40). Output power from a 515 nm argon-ion laser line (Melles Griot) was adjusted and measured at the objective with a FieldMax II-TO power meter (Coherent). Emission was collected with detector slit settings of 530–630 nm. Raw data were collected with the FV1000 FluoView software and then exported to Excel for processing.

Organized Smooth Endoplasmic Reticulum Live-Cell Assay

HeLa (CCL-2) cells were cultured in DMEM supplemented with 12.5% FBS. The cells were seeded onto 35-mm culture dishes containing 18 × 18 mm glass coverslips. Approximately 24 hr after being seeded, the cells were transfected with 1 μg of the CytERM fusion DNA using Effectene (QIAGEN) and maintained in a 5% CO_2 incubator for 24 hr before counting. Transient transfections were visually assayed on an Olympus IX71 inverted microscope equipped with an LCPlanFluor 40× dry objective (NA = 0.60). The assay was performed by counting the total number of cells in the field of view, then counting the total number of cells with morphologically normal ER with no stacked cisternae "whorls." Multiple viewfields were counted until a total of 10,000 cells was reached. The number of cells displaying smooth ER morphology was divided by the total number of cells to determine the percentage of "normal morphology" cells for each FP fusion.

Statistical Analysis

All error bars represent SD.

ACCESSION NUMBERS

The GenBank accession number for mPapaya1 reported in this paper is KF309175.

SUPPLEMENTAL INFORMATION

Supplemental Information includes four figures and two tables and can be found with this article online at http://dx.doi.org/10.1016/j.chembiol.2013.08.008.

ACKNOWLEDGMENTS

We are grateful to Allele Biotechnology for the kind gift of the codon optimized zFP538 gene. The mammalian expression plasmid encoding CytERM-mEGFP is courtesy of Professor Erik Snapp at the Albert Einstein College of Medicine. We thank the University of Alberta MBSU and Christopher W. Cairo for technical assistance. Funding support was provided by CIHR (NHG 99085 and MOP 123514) and NSERC (to R.E.C.). W.Z. is supported by a scholarship from Alberta Innovates. R.E.C. holds a Tier II Canada Research Chair. The University of Alberta and Allele Biotechnology have filed a provisional US patent application on mPapaya1.

Received: July 13, 2013
Revised: August 23, 2013
Accepted: August 28, 2013
Published: October 3, 2013

REFERENCES

Ai, H.W., Henderson, J.N., Remington, S.J., and Campbell, R.E. (2006). Directed evolution of a monomeric, bright and photostable version of Clavularia cyan fluorescent protein: structural characterization and applications in fluorescence imaging. Biochem. J. *400*, 531–540.

Campbell, R.E., Tour, O., Palmer, A.E., Steinbach, P.A., Baird, G.S., Zacharias, D.A., and Tsien, R.Y. (2002). A monomeric red fluorescent protein. Proc. Natl. Acad. Sci. USA *99*, 7877–7882.

Cheng, Z., and Campbell, R.E. (2006). Assessing the structural stability of designed beta-hairpin peptides in the cytoplasm of live cells. ChemBioChem *7*, 1147–1150.

Costantini, L.M., Fossati, M., Francolini, M., and Snapp, E.L. (2012). Assessing the tendency of fluorescent proteins to oligomerize under physiologic conditions. Traffic *13*, 643–649.

Ding, Y., Ai, H.W., Hoi, H., and Campbell, R.E. (2011). FRET-based biosensors for multiparameter ratiometric imaging of Ca^{2+} dynamics and caspase-3 activity in single cells. Anal. Chem. *83*, 9687–9693.

Griesbeck, O., Baird, G.S., Campbell, R.E., Zacharias, D.A., and Tsien, R.Y. (2001). Reducing the environmental sensitivity of yellow fluorescent protein. Mechanism and applications. J. Biol. Chem. *276*, 29188–29194.

Gurskaya, N.G., Verkhusha, V.V., Shcheglov, A.S., Staroverov, D.B., Chepurnykh, T.V., Fradkov, A.F., Lukyanov, S., and Lukyanov, K.A. (2006). Engineering of a monomeric green-to-red photoactivatable fluorescent protein induced by blue light. Nat. Biotechnol. *24*, 461–465.

Henderson, J.N., Ai, H.W., Campbell, R.E., and Remington, S.J. (2007). Structural basis for reversible photobleaching of a green fluorescent protein homologue. Proc. Natl. Acad. Sci. USA *104*, 6672–6677.

Hoi, H., Shaner, N.C., Davidson, M.W., Cairo, C.W., Wang, J., and Campbell, R.E. (2010). A monomeric photoconvertible fluorescent protein for imaging of dynamic protein localization. J. Mol. Biol. *401*, 776–791.

Ilagan, R.P., Rhoades, E., Gruber, D.F., Kao, H.T., Pieribone, V.A., and Regan, L. (2010). A new bright green-emitting fluorescent protein—engineered monomeric and dimeric forms. FEBS J. *277*, 1967–1978.

Karasawa, S., Araki, T., Nagai, T., Mizuno, H., and Miyawaki, A. (2004). Cyan-emitting and orange-emitting fluorescent proteins as a donor/acceptor pair for fluorescence resonance energy transfer. Biochem. J. *381*, 307–312.

Matz, M.V., Fradkov, A.F., Labas, Y.A., Savitsky, A.P., Zaraisky, A.G., Markelov, M.L., and Lukyanov, S.A. (1999). Fluorescent proteins from nonbioluminescent Anthozoa species. Nat. Biotechnol. *17*, 969–973.

Miyawaki, A., Llopis, J., Heim, R., McCaffery, J.M., Adams, J.A., Ikura, M., and Tsien, R.Y. (1997). Fluorescent indicators for Ca^{2+} based on green fluorescent proteins and calmodulin. Nature *388*, 882–887.

Nagai, T., Ibata, K., Park, E.S., Kubota, M., Mikoshiba, K., and Miyawaki, A. (2002). A variant of yellow fluorescent protein with fast and efficient maturation for cell-biological applications. Nat. Biotechnol. *20*, 87–90.

Ormö, M., Cubitt, A.B., Kallio, K., Gross, L.A., Tsien, R.Y., and Remington, S.J. (1996). Crystal structure of the Aequorea victoria green fluorescent protein. Science *273*, 1392–1395.

Pakhomov, A.A., and Martynov, V.I. (2011). Probing the structural determinants of yellow fluorescence of a protein from Phialidium sp. Biochem. Biophys. Res. Commun. *407*, 230–235.

Patterson, G.H., Piston, D.W., and Barisas, B.G. (2000). Förster distances between green fluorescent protein pairs. Anal. Biochem. *284*, 438–440.

Pletneva, N.V., Pletnev, S.V., Chudakov, D.M., Tikhonova, T.V., Popov, V.O., Martynov, V.I., Wlodawer, A., Dauter, Z., and Pletnev, V.Z. (2007). [Three-dimensional structure of yellow fluorescent protein zYFP538 from Zoanthus sp. at the resolution 1.8 angstrom]. Bioorg. Khim. *33*, 421–430.

Remington, S.J., Wachter, R.M., Yarbrough, D.K., Branchaud, B., Anderson, D.C., Kallio, K., and Lukyanov, K.A. (2005). zFP538, a yellow-fluorescent protein from Zoanthus, contains a novel three-ring chromophore. Biochemistry *44*, 202–212.

Shagin, D.A., Barsova, E.V., Yanushevich, Y.G., Fradkov, A.F., Lukyanov, K.A., Labas, Y.A., Semenova, T.N., Ugalde, J.A., Meyers, A., Nunez, J.M., et al. (2004). GFP-like proteins as ubiquitous metazoan superfamily: evolution of functional features and structural complexity. Mol. Biol. Evol. *21*, 841–850.

Shaner, N.C., Campbell, R.E., Steinbach, P.A., Giepmans, B.N., Palmer, A.E., and Tsien, R.Y. (2004). Improved monomeric red, orange and yellow fluorescent proteins derived from Discosoma sp. red fluorescent protein. Nat. Biotechnol. *22*, 1567–1572.

Shaner, N.C., Steinbach, P.A., and Tsien, R.Y. (2005). A guide to choosing fluorescent proteins. Nat. Methods *2*, 905–909.

Shaner, N.C., Lin, M.Z., McKeown, M.R., Steinbach, P.A., Hazelwood, K.L., Davidson, M.W., and Tsien, R.Y. (2008). Improving the photostability of bright monomeric orange and red fluorescent proteins. Nat. Methods *5*, 545–551.

Shaner, N.C., Lambert, G.G., Chammas, A., Ni, Y., Cranfill, P.J., Baird, M.A., Sell, B.R., Allen, J.R., Day, R.N., Israelsson, M., et al. (2013). A bright monomeric green fluorescent protein derived from Branchiostoma lanceolatum. Nat. Methods *10*, 407–409.

Snapp, E.L., Hegde, R.S., Francolini, M., Lombardo, F., Colombo, S., Pedrazzini, E., Borgese, N., and Lippincott-Schwartz, J. (2003). Formation of stacked ER cisternae by low affinity protein interactions. J. Cell Biol. *163*, 257–269.

Yanushevich, Y.G., Staroverov, D.B., Savitsky, A.P., Fradkov, A.F., Gurskaya, N.G., Bulina, M.E., Lukyanov, K.A., and Lukyanov, S.A. (2002). A strategy for the generation of non-aggregating mutants of Anthozoa fluorescent proteins. FEBS Lett. *511*, 11–14.

Zacharias, D.A., Violin, J.D., Newton, A.C., and Tsien, R.Y. (2002). Partitioning of lipid-modified monomeric GFPs into membrane microdomains of live cells. Science *296*, 913–916.

Zagranichny, V.E., Rudenko, N.V., Gorokhovatsky, A.Y., Zakharov, M.V., Shenkarev, Z.O., Balashova, T.A., and Arseniev, A.S. (2004). zFP538, a yellow fluorescent protein from coral, belongs to the DsRed subfamily of GFP-like proteins but possesses the unexpected site of fragmentation. Biochemistry *43*, 4764–4772.

